



ORIGINAL ARTICLE

Structural response of high strength concrete beams using fiber reinforced polymers under reversed cyclic loading

Mohamed T. Elshazli^a, Nick Saras^b, Ahmed Ibrahim^{a,*}

^aDepartment of Civil and Environmental Engineering, University of Idaho, Moscow, ID, 83844, USA

^bHorrocks Engineers, 2775 W. Navigator Dr., Suite 210, Meridian, ID 83642, USA

*Corresponding Author: Ahmed Ibrahim, aibrahim@uidaho.edu

Abstract: This paper investigates the response of high strength concrete (HSC) beams subjected to reversed cyclic loading using carbon fiber-reinforced polymer (CFRP), glass fiber-reinforced polymers (GFRP), and hybrid FRP/steel bars as bottom tensile reinforcement. Five HSC beams with a rectangular cross-section were prepared and poured using with a 28-day concrete compressive strength of 60 MPa (8.7 ksi). A displacement-controlled reversed cyclic loading has been applied to all the beams. The test setup has been designed to represent seismic effect on structures. Flexural capacity, concrete and reinforcement steel strains, cracking behavior, and ductility results were obtained. The hybrid steel/FRP has shown an improved performance in terms of flexural capacity, strains, and ductility. While the inclusion of FRP grids reduces the flexural capacity, this can be improved by adding more layers of FRP. Overall, the nominal moment of the hybrid sections were the highest between all beams. The ACI 318 code's empirical equations showed close results in terms of the tensile strength of the FRP. The ACI 440R has shown overestimated nominal moment values compared to the experimental results.

Keywords: High strength concrete; carbon fiber; glass fiber; reversed cyclic

1 Introduction

Over many years, High Strength Concrete (HSC) was considered the main building material used in structures. The aging problem of infrastructure is increasing and solutions to extend the service life need to be found. Corrosion is one of the main leading causes of structures' aging, where it accelerates the deterioration process. The very popular signs of steel corrosion is delamination and concrete spalling. Alternative solutions need to be more investigated to mitigate such corrosion problems in concrete structures.

The addition of Fiber-Reinforced Polymer (FRP) in HSC is a one of the promising solution to avoid corrosion problems [1-6]. In the last 25 years, FRP has been widely used in different civil engineering applications [7-10]. Various commercial kinds of FRP are available in the market for implementation in concrete structures such as bars, grids and FRP wraps [11-12]. Those FRP types might be used as internal reinforcement or used externally to strengthen damaged concrete elements. FRP is distinguished from conventional steel due to its corrosion resistance and extremely high tensile strength [13-16]. The behavior of conventional steel bars is usually linear up to the elastic limit, followed by yielding and strain hardening and then strain softening and failure. The FRP is a brittle material that has linear elastic behavior up to failure. The usage of both conventional steel bars and FRP



bars/grids might be an advantage of combining the two behaviors to enhance the overall concrete element's strength and ductility

Most of the published research [9, 11, 14-15, 17-19] was focused on the performance of reinforced concrete elements reinforced by FRP bars under monotonic loading. The inclusion of FRP grids in high strength concrete elements is very limited and the behavior of such beams under reverse cyclic loading is also limited and need more investigation. The cyclic loading is a type of loading protocols that mimic the seismic forces' effect on a concrete member. The reason of performing cyclic is due to the difficulty and cost of investigating such behavior using a shaking table.

Fiber-Reinforced Polymer (FRP) are considered high-performance materials with superior characteristics, such as; light weight, high tensile strength, fatigue resistance, corrosion resistance, and heat insulation. Recently, FRP has been utilized in many civil engineering applications, for instance, bridges, marine constructions, and underground infrastructures [20]. Four types of FRP are commonly used in structures applications (Carbon FRP, Glass FRP, Aramid FRP, and Basalt FRP). These FRP materials are distinguished by their corrosion resistance, making them a good substitute for conventional steel reinforcement. The physical and mechanical properties of the different FRP materials compared to conventional steel are shown in Table 1. The reduced density of FRP leads to a reduced weight, almost 1/5 compared to conventional steel. Although FRP has demonstrated a high tensile strength, the elongation percentage is low, resulting in a brittle failure. Moreover, the elastic modulus of FRP usually is lower than that of steel (except for some CFRP, which has a high elastic modulus).

Table 1. Physical and mechanical properties of FRP materials compared to conventional steel [20]

Material	Unit Weight (g/cm ³)	Longitudinal coefficient of thermal expansion (10 ⁻⁶ /°C)	Tensile strength (MPa)	Elastic Modulus (GPa)	Ultimate elongation (%)
CFRP	1.50 - 1.60	-9.0 - 0.0	600 - 3690	120 - 580	0.5 - 1.7
GFRP	1.25 - 2.10	6.0 - 10.0	483 - 1600	35 - 51	1.2 - 3.1
AFRP	1.25 - 1.40	-6.0 - 2.0	1720 - 2540	41 - 125	1.9 - 4.4
BFRP	1.90 - 2.10	9.0 - 12.0	600 - 1500	50 - 65	1.2 - 2.6
Steel	7.85	11.7	483 - 690	200	6.0- 12.0

Various research work has been conducted to investigate the non-corrosive behavior of FRP when used as reinforcement in ordinary concrete. The FRP has been used in different forms (bars, tubes, sheets, plates, discrete needles, and grids) [21]. The literature indicated that GFRP and CFRP are the most common FRP reinforcement materials. GFRP has been examined under different environmental conditions to investigate its long-term performance. Aggressive environments were considered, such as; normal and high alkaline and saline solutions [22-26], seawater [27-34], and acids [23]. In addition, elevated temperature has been applied to accelerate the reactions [22, 25, 30]. The results showed a maintained high tensile strength of the GFRP, and no chemical degradation was detected. In addition, it was found that the degradation level depends on the conditioning temperature rather than the conditioning duration [31-32].

To avoid the CFRP-reinforced concrete beams' sudden brittle failure, most design codes suggest designing the sections as under-reinforced sections [14, 31-37]. The CFRP under-reinforced sections have experienced a less catastrophic failure with excessive deflection and wide cracks due to the lower elasticity modulus of CFRP compared to the conventional steel [38-43]. Although the modulus of elasticity of CFRP is lower than steel, it is four to five times higher than the elastic modulus of GFRP (See **Table 1**). In return, CFRP beams have shown higher flexural strength compared to GFRP beams. However, the behavior of concrete beams reinforced by CFRP and GFRP under different conditions is still under study, GFRP reinforced behavior has experienced higher deflection and wider cracks than conventional steel reinforcement [42]. The low elastic modulus of GFRP, compared to steel, results in low post-cracking stiffness compared to conventional reinforced concrete beams [42].

Most of the stakeholder and owners of structures have reported that the initial cost of FRP is an overburden to the overall project cost. However, if the overall cost of labor and materials of both steel and FRP have been compared. The FRP might win in certain cases depending on the complexity of the project, the construction time, maintenance cost and many other factors [44-45]. The FRP bars showed

very effective cost-saving (57%) when implemented in bridge deck compared to normal steel reinforcement, Berg et al. [13]. The initial cost of FRP bars might be high as 60%, Berg et al. [13]. In addition, the maintenance cost through the service life of the structure could be eliminated by using FRP reinforcement.

Cyclic load is defined as a repeated load (reversed cyclic) that includes push and pull of the structural element, [46-47]. Cyclic loads creates a state of stress that produces fatigue to the element and the element might fail at a stress value that is less than its ultimate stress. Fatigue analysis might be performed under high or low cyclic loads. High cyclic fatigue might include millions of cycles applied to the concrete element, whereas low cyclic is performed under few limited number of cycles similar to the one conducted in this study. Cyclic load is applied to the element in a short period of time, which is considered a dynamic load that mimic seismic loads. Limited number of studies have been performed to study the response of HSC under reversed-cyclic loading.

Various studies [48-50] have reported results related to the behavior of high strength concrete reinforced by normal and FRP bars under cyclic loading. High strength concrete cantilever beams have been tested under fatigue loads, Fang et. al. [50]. The study showed that the high strength concrete could offer a better ultimate loading capacity with better energy absorption. In addition, other study showed that normal weight concrete is better than high strength concrete in terms of ductility under cyclic loads, Xue et. al. [51]. The hysteretic behavior of high strength concrete beams under cyclic loads is much better than normal weight concrete, Xiao et. al. [52]. The implementation of FRP grids as reinforcement in high strength concrete under cyclic loading is very limited. The behavior of normal weight concrete cantilever beams reinforced with FRP grids has been investigated by Sharbatdar et. al. [53]. The results showed that the beams flexural strength have been degraded progressively due to cracking.

Overall, FRP has shown promising properties to be used as an alternative sustainable solution compared to conventional steel reinforcement. The main advantages of FRP are their high strength-to-weight ratio and high corrosion resistance. Much research work has been performed on the flexural behavior of FRP and hybrid FRP and steel reinforcement. Limited research has been conducted on the reverse-cyclic analysis of FRP and hybrid FRP/steel reinforced HSC beams. This paper aims to experimentally investigate the structural response of HSC beams subjected to reversed cyclic loading in the case of using CFRP, GFRP, and hybrid FRP/steel reinforcement. This work introduces the behavior of the HSC beams reinforced under the grid action of CFRP and GFRP. Most of the works cited have used bars only. This study shows a preliminary behavior of HSC beams reinforced with such grids under reverse cyclic loads.

Table 2. Details of beam specimens

Type	Beam ID	Bottom Reinforcement	RFT. Area (mm ²)
Control Specimen	ST	Two 16 mm Grade 60 reinforcement	400
CFRP Grid	CF	1 row - CFRP grid	200
GFRP Grid	GF	1 row - GFRP grid	160
CFRP + Steel	CF/ST	Two 16 mm Grade 60 reinforcement + 1 row - CFRP grid	600
GFRP + Steel	GF/ST	Two 16 mm Grade 60 reinforcement + 1 row - GFRP grid	560

2 Experimental Program

2.1 Test Specimens

This paper aimed at investigating the response of HSC beams subjected to low- cyclic fatigue loading by using CFRP, GFRP, and hybrid FRP/steel bars as tensile reinforcement. Five high strength concrete beams were prepared and cast using concrete with a 28-day compressive strength of 60 MPa (8.7 ksi). All beams had a rectangular cross-section of 200 mm (8 in.) wide × 230 mm (9 in.) high with 2140 mm (7 ft.) long. The control beam was reinforced using two 16 mm diameter, high yield strength deformed bars Grade 60 (with a yield strength of 415 N/mm²) as bottom reinforcement. Carbon fiber and glass fiber grids were used as bottom reinforcement for CF and GF specimens. The last two beams were reinforced using conventional steel and FRP grids as hybrid bottom reinforcement. The details of the specimens are shown in **Table 2**. Finally, all beams used two 10 mm diameter Grade 60 steel rebar

for top reinforcement and stirrups, spaced at 200 mm. Clear cover for reinforcement was maintained at 25 mm at all sides.

2.2 Materials

A single HSC mix with an actual 28-day compressive strength of 60 MPa (8.7 ksi) has been used in all the specimens. The target compressive strength provided to the concrete plant was 48.2 MPa (7 ksi). The coarse aggregate used was dolomite with a nominal particle size of 19 mm (0.75 in.), and the fine aggregate was natural sand. Type II Portland cement with a specific gravity of 3.15 and conforming to the requirements of the ASTM C150 was used. The design of HSC mixes always requires water-reducing agents to maintain strength while keeping the water-to-cement ratio low and providing a more workable concrete. This was obtained using an air-entrainer (Daravair) and a water-reducing agent (Daracem) as admixtures. As a result, a water-to-cement ratio of 0.33 with a slump value of 100 mm (4 in.) was produced. The details of the concrete mixture are shown in **Table 3**.

Table 3. Concrete mix proportions

Cement kg/m ³ (lbs/yd ³)	Water lit./m ³ (gal/yd ³)	Fine Agg. kg/m ³ (lbs/yd ³)	Coarse Agg. kg/m ³ (lbs/yd ³)	Air-entrainer kg/m ³ (oz/yd ³)	Water reducing agent kg/m ³ (oz/yd ³)
500.00 (842)	163.39 (33)	860.25 (1450)	1023.40 (1725)	0.116 (3)	1.934 (50)

NEFMAC (New Fiber Composite Material for Reinforcing Concrete) FRP glass and carbon fibers were used in this study [54-56]. The carbon and glass fibers had a fiber volume of approximately of 40%. The grid was produced to form a 2D orthogonal grid with symmetrical mechanical properties, as shown in **Fig. 1**. The properties of the used FRP are shown in **Table 4**.

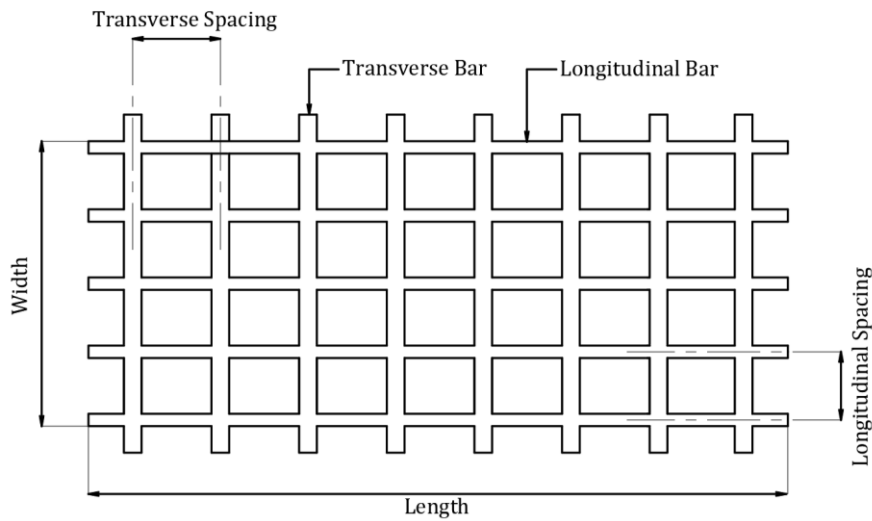


Fig. 1. FRP grid

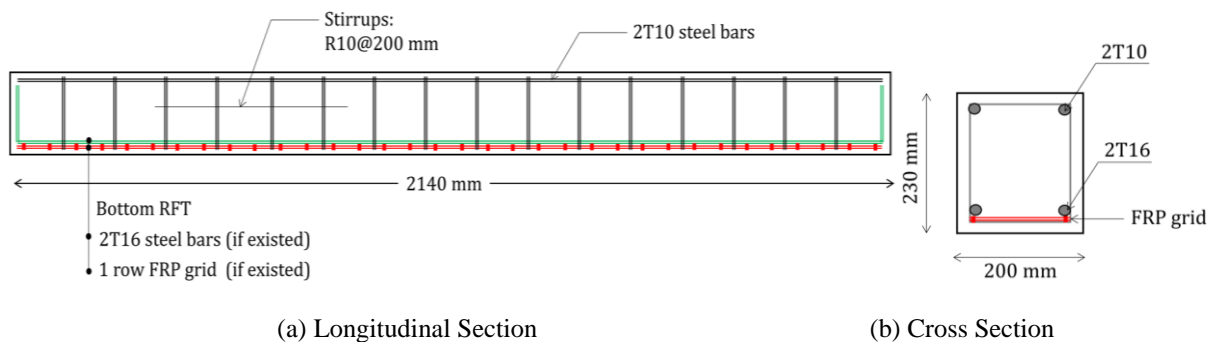


Fig. 2. Typical beam reinforcement details

Table 4. Properties of the Steel and FRP bars

Reinforcement Type	Area mm ² (in ²)	Tensile Strength N/mm ² (ksi)	Elastic Modulus N/mm ² (ksi)	Yield Stress N/mm ² (ksi)	Strain at Break %	Weight kg/m (lb/ft)
16 mm Grade 60	200 (0.310)	690 (100)	199,950 (29,000)	415 (60)	0.14-0.25	1.55 (1.043)
NEFMAC CFRP grid	100 (0.155)	1200 (174)	99,975 (14,500)	N/A	0.50-1.90	0.78 (0.525)
NEFMAC GFRP grid	80 (0.122)	600 (87)	29,995 (4,350)	N/A	1.20-3.10	0.43 (0.292)

2.3 Instrumentation, test setup, and loading program

All formwork has been prepared and manufactured using available wood achieving a concrete cover of 25 mm on all sides of the beams. **Fig. 2** shows the reinforcement details of the beams and **Fig. 3** shows the hybrid FRP/steel reinforcement cages. The test setup has been designed to simulate the forces and boundary conditions that could happen during a seismic action. The two ends of the beam were fixed, as shown in **Fig. 4**.



Fig.3. Hybrid FRP/steel reinforcement cage; a) CF/ST reinforcement, b) GF/ST reinforcement

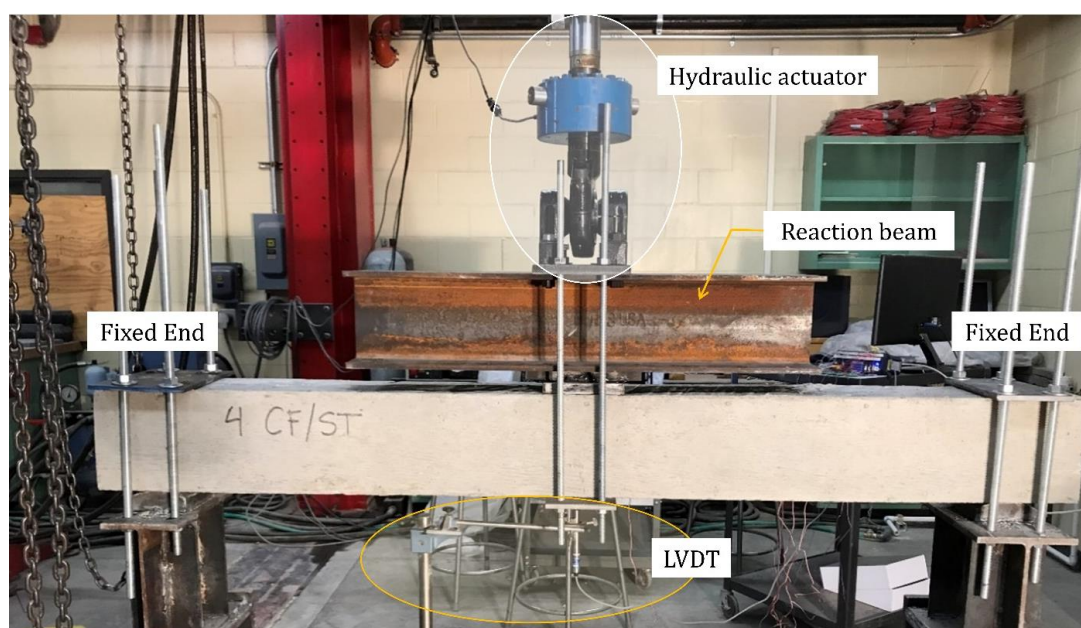


Fig.4. Test setup

Reversed cyclic loading has been applied to the mid-span using a hydraulic actuator with a 2000 kN capacity. A steel reaction beam was used to apply the load at the midspan. A load cell has been used to record the applied load in kN. The load cell has a maximum capacity of 225 kN (50,000 lbf.). An LVDT has been used to measure the deflection at midspan. Three steel strain gauges were attached to the reinforcement and stirrups at the midspan of each beam. In addition, one strain gauge has been externally attached to the midspan of the concrete. Test setup details are shown in **Fig.4**. The reverse cyclic system is controlled by Shore Western System. The reversed cyclic loading history is shown in **Fig.5**. Displacement controlled loading protocol has been applied to all specimens. This loading protocol has been designed based on multiple data found in the literature.

3 Experimental results and discussion

The parameters that have been considered were the flexural capacity, concrete and reinforcement strains, cracking behavior, and ductility index. A summary of the experimental results is shown in **Table 5**.

Table 5. Summary of the experimental results

Beam ID	Max. Load		Corresponding Displacement		Ultimate Strain			Ductility Index
	Push kN (kips)	Pull kN (kips)	Push mm (in.)	Pull mm (in.)	Steel mm/mm	FRP mm/mm	Concrete mm/mm	
ST	109.16 (24.54)	55.60 (12.50)	16.52 (0.6504)	18.66 (0.7231)	0.03341	N/A	0.03127	2.64
CF	91.63 (20.60)	36.20 (8.14)	19.26 (0.7585)	16.06 (0.6323)	N/A	0.03570	0.00002	N/A
GF	44.93 (10.10)	27.18 (6.11)	18.23 (0.7178)	16.43 (0.6470)	N/A	0.03362	0.00049	N/A
CF/ST	126.95 (28.54)	40.61 (9.13)	19.15 (0.7541)	15.98 (0.6294)	0.00481	0.03373	0.00082	1.94
GF/ST	107.02 (24.06)	30.02 (6.75)	19.72 (0.7764)	18.77 (0.7393)	0.00586	0.03375	0.00022	1.70

3.1 Failure Load and Ductility Index

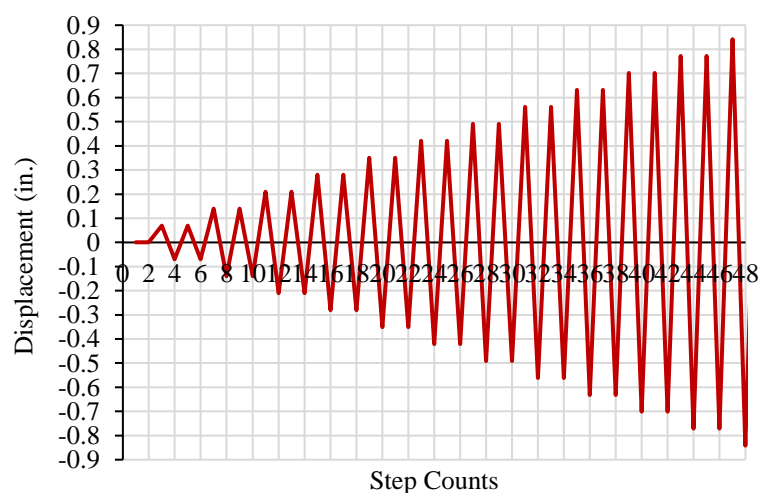


Fig. 5. The reversed cyclic loading protocol

The specimens were tested under cyclic loading using a displacement-controlled regime. **Fig. 6** shows the peak load results for all specimens under the reversed cyclic loading. The controlled beam with the conventional reinforcement had shown a peak load of 109.16 kN (24.54 kips) when subjected to the cyclic loading protocol illustrated in **Fig. 5**. The use of FRP only as bottom reinforcement reduced

the flexural capacity by 16% for CFRP grids and 58% for GFRP grids compared to the control beam. Compared to the control beam, the hybrid system has improved flexural capacity, especially for the CFRP, with an increase in flexural capacity by 17%.

Overall, beams with hybrid reinforcement (FRP grids and conventional steel) have shown the highest flexural capacity and ductility, compared to the beams reinforced with FRP only. Beams prepared with hybrid reinforcement did show an increase in the flexural capacity. The weight of the steel bottom reinforcement used in the control specimen is roughly equal to 3.3 kilograms (7.3 pounds). At the same time, the carbon fiber and glass fiber grids weigh approximately 1.7 kg (3.7 pounds) and 0.9 kg (2.0 pounds), respectively. That’s why specimens containing FRP only did not show superiority in the flexural capacity compared to the control beam. However, the flexural capacity can be increased by adding more layers/grids of the FRP.

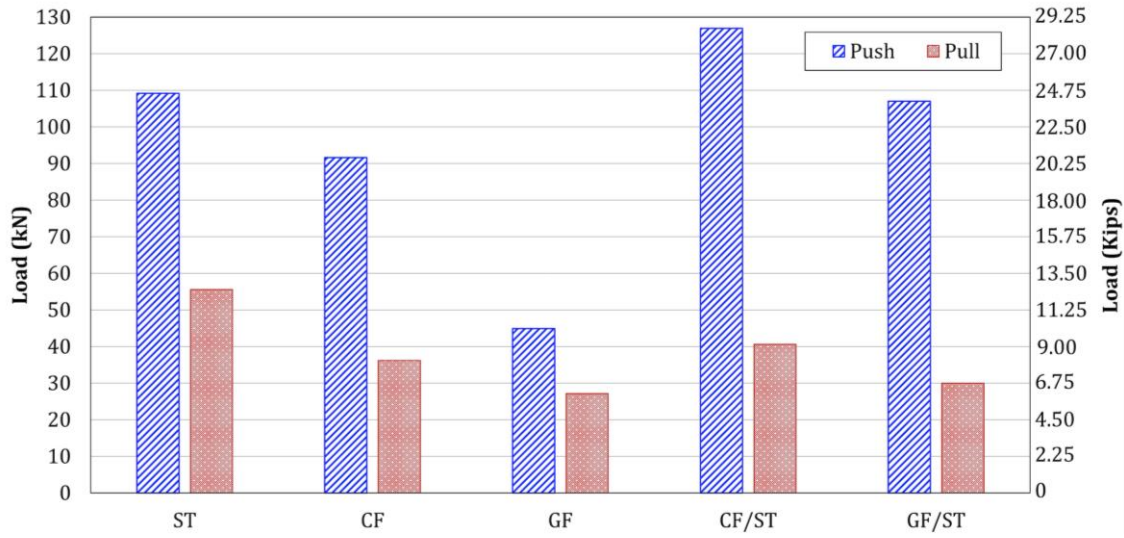


Fig. 6. Peak load results

Fig. 7 to Fig. 11 show the load-displacement Hysteresis curves. The improved flexural capacity due to the hybrid reinforcement can be seen in Figure 10 for CFRP and Fig. 11 for GFRP. Load displacement failure envelopes were developed, Fig. 12 to Fig. 16. The green highlighting region illustrates the ductility area using the strain values obtained for the steel and FRPs during the test. The first bound of the box corresponds to the load where the reinforcement yield (δ_y). The second bound of the box corresponds to the ultimate reinforcement strength (δ_u). These two values were used to obtain the ductility index (μ) illustrated in Table 5.

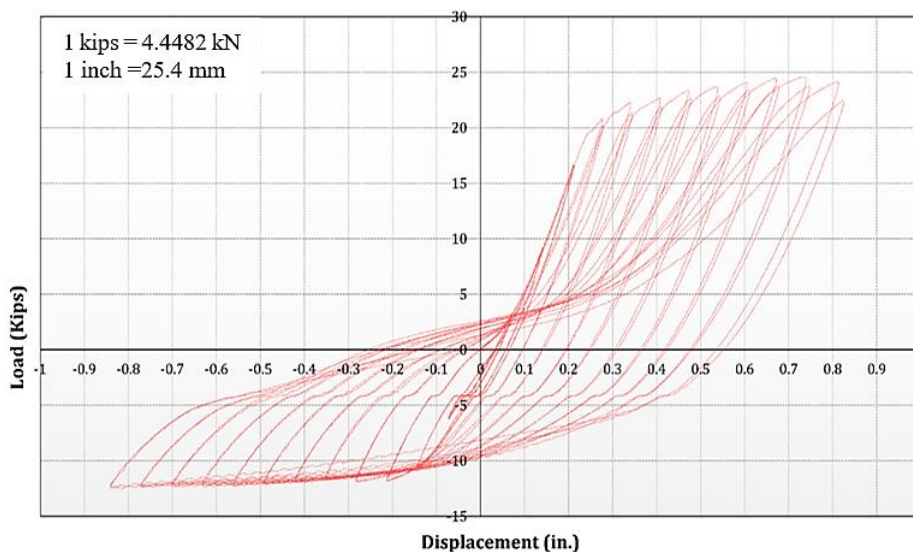


Fig. 7. Load-Displacement Hysteresis curve for the control beam (ST)

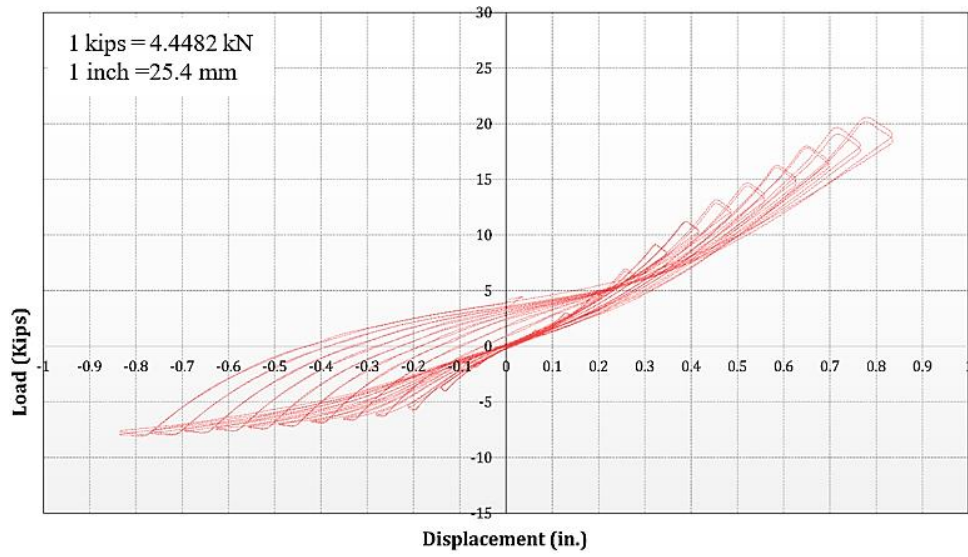


Fig. 8. Load-Displacement Hysteresis curve for the CF beam

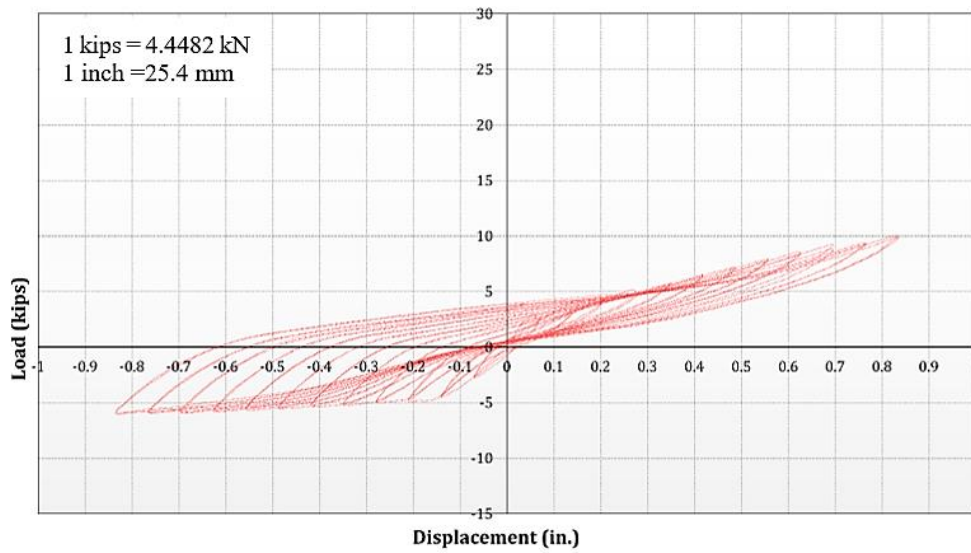


Fig. 9. Load-Displacement Hysteresis curve for the GF beam

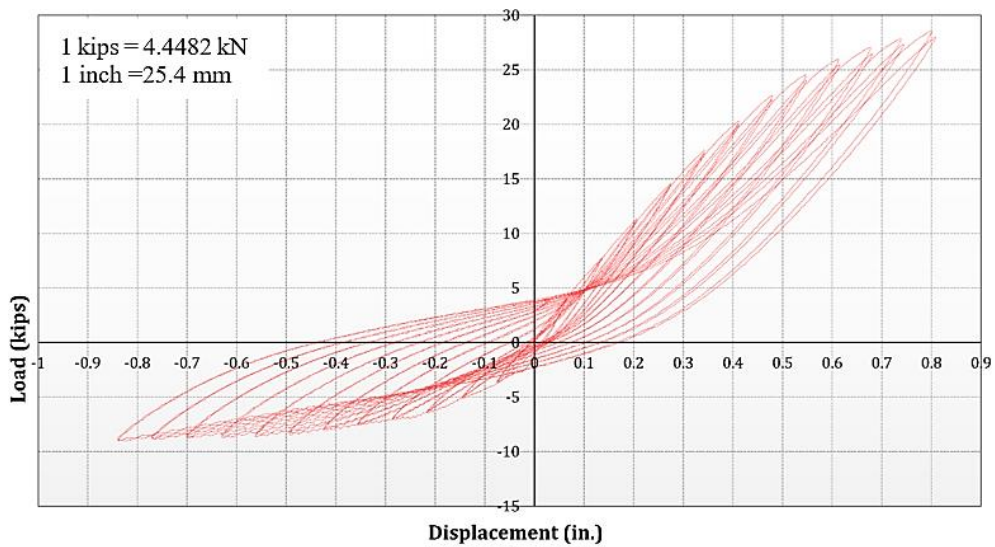


Fig.10. Load-Displacement Hysteresis curve for the Hybrid (ST and CF) beam

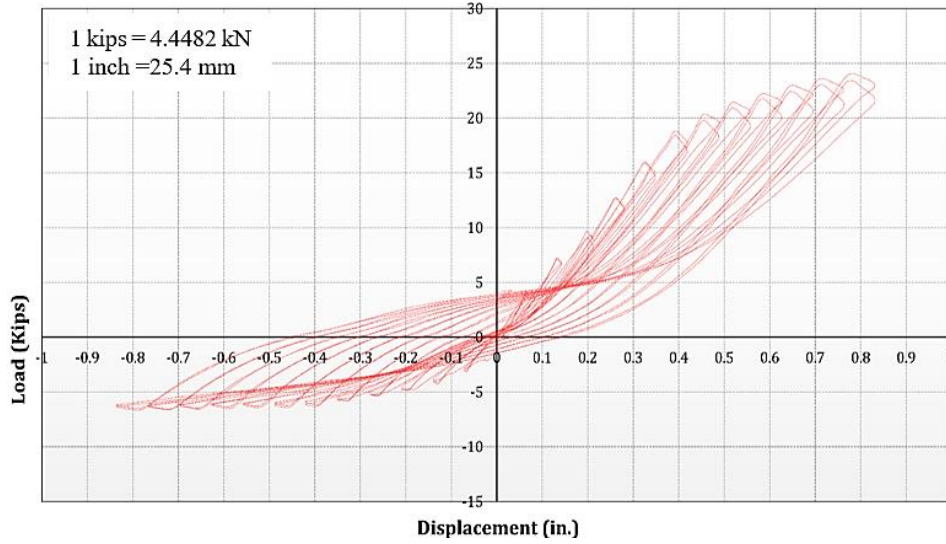


Fig. 11. Load-Displacement Hysteresis curve for the Hybrid (ST and GF) beam

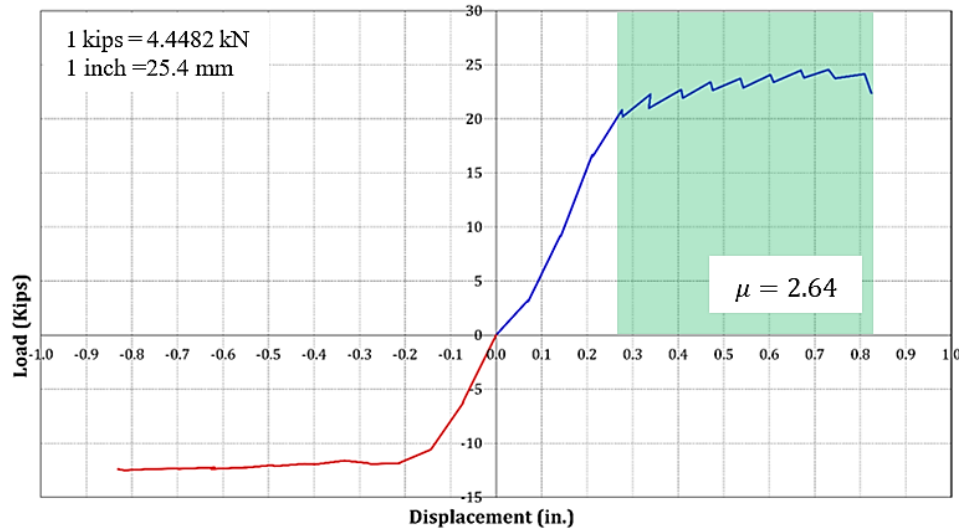


Fig. 12. Load-Displacement failure envelope for the control beam (ST)

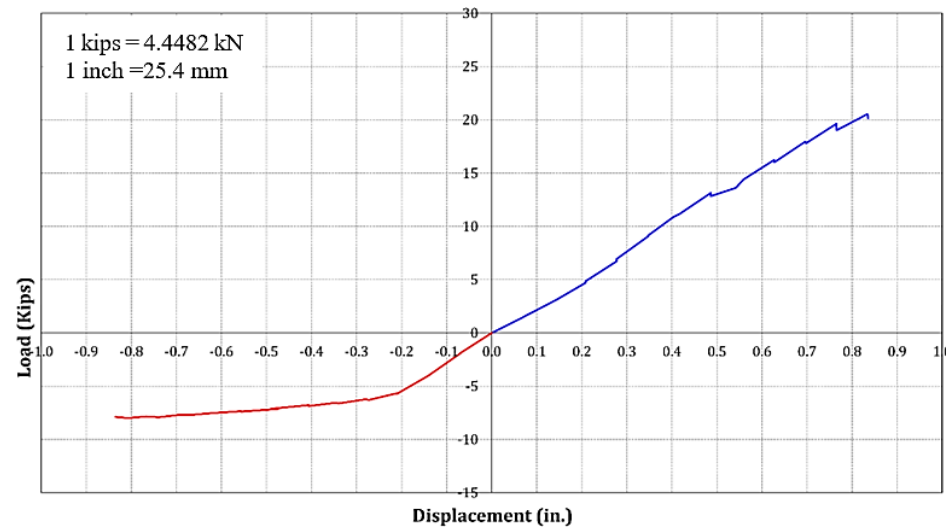


Fig. 13. Load-Displacement failure envelope for the CF beam

The ratio of the maximum deflection to the deflection corresponds to the yield stress is defined as the Ductility index. The maximum deflection is the value of the beams' vertical displacement where the

beam would not be able to resist further load. For CF and GF beams, there was no ductility index due to the brittleness behavior of the FRP, as shown in **Fig. 13** and **Fig. 14**. However, hybrid reinforcement has shown an acceptable ductility behavior, **Fig. 15** and **Fig. 16**. **Fig. 17** shows an overall comparison of load-deflection envelopes for all beams.

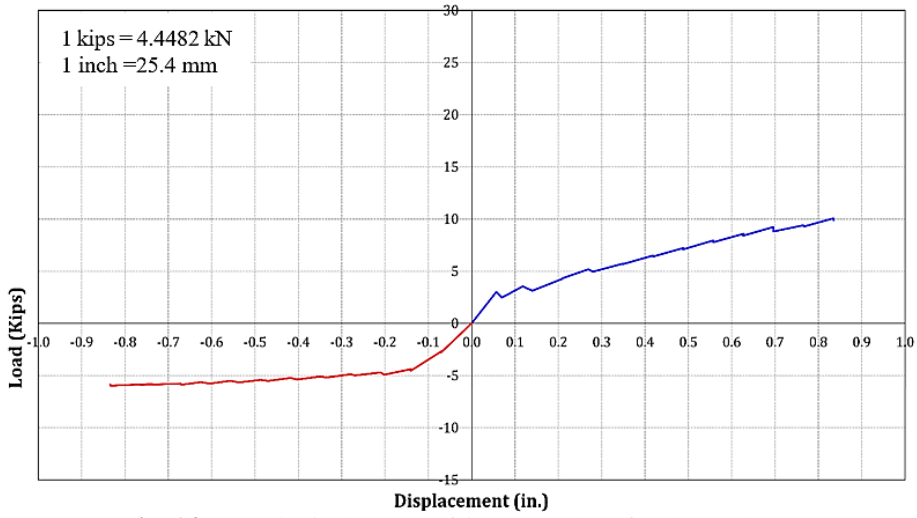


Fig. 14. Load-Displacement failure envelope for the GF beam

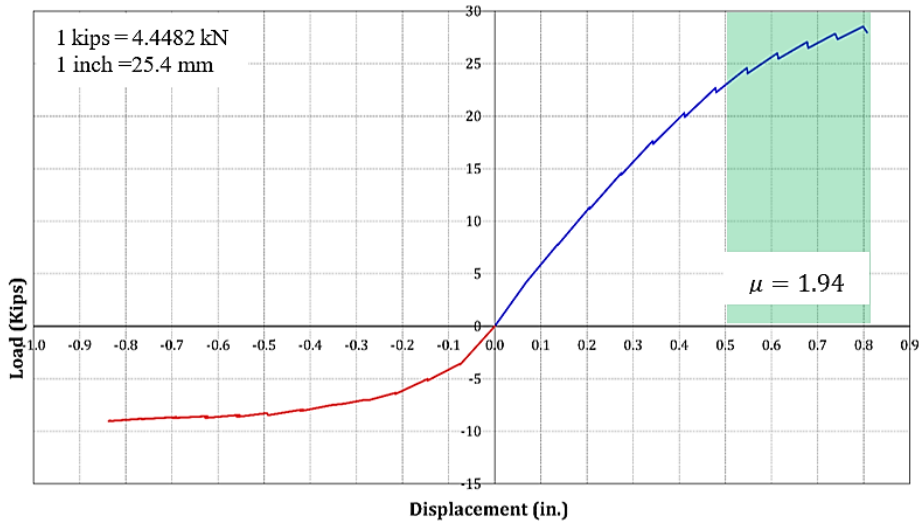


Fig. 15. Load-Displacement failure envelope for the Hybrid (ST/CF) beam

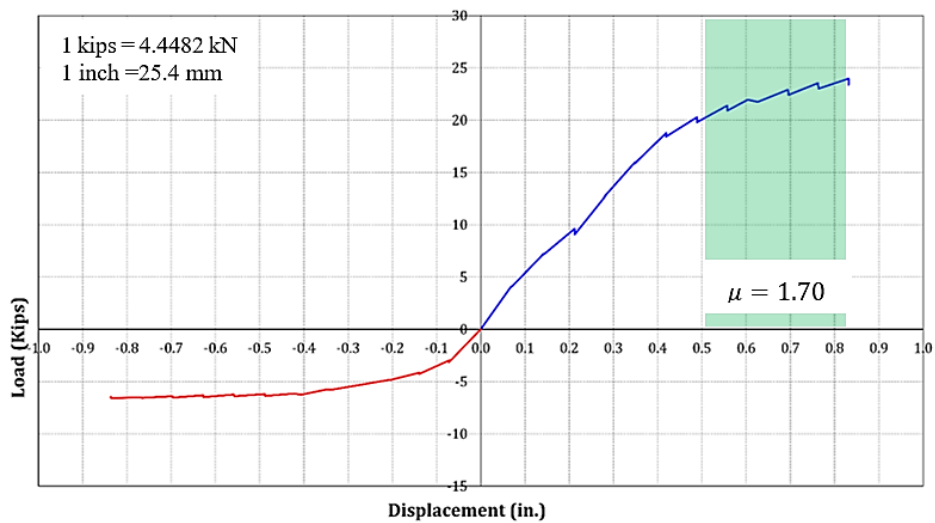


Fig. 16. Load-Displacement failure envelope for the Hybrid (ST/GF) beam

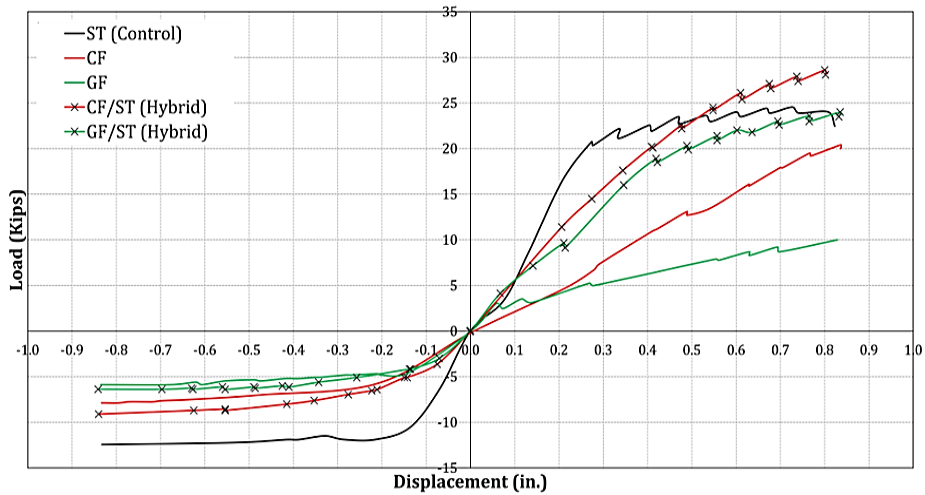


Fig. 17. Load-Displacement failure envelopes for all beams

3.2 Strain

All beams have experienced flexural failure, where reinforcement reaches its yield strength before the failure of the concrete. For the control beam, it was observed that the main steel has yielded before concrete. The steel strain was 0.0334, corresponding to a load of 104 kN (23.4 kips). For the FRP specimens, flexural cracks were developed at the midspan and increased until the FRP reached the ultimate strain and was delaminated. **Fig. 18** to **Fig. 22** show the flexural failure shapes of the specimens.



Fig.18. Flexural failure of the control (ST) beam



Fig. 19. Flexural failure of the (CF) beam



Fig. 20. Flexural failure of the (GF) beam

For the hybrid reinforcement (CF/ST) beam, the CFRP was delaminated at a load of 109.43 kN (24.6 kips) before the yielding of the steel bars. The delamination has occurred at a strain value of 0.0336. The dominant failure of the beam was due to flexure, as shown in **Fig. 19**. The steel bars have reached its yield strength after the delamination of the CFRP at a strain value of 0.0022 in the first cycle

and corresponding to a load of 110.76 kN (24.9 kips). On the other hand, the steel in the hybrid reinforcement (GF/ST) beam first yielded a strain value of 0.0044, corresponding to a load of 90 kN (20.3 kips). Then the GFRP grid showed delamination at a strain value of 0.0338, corresponding to a load of 95 kN (21.4 kips). As mentioned earlier, these strain values and observations were used to obtain the ductility index.



Fig. 21. Flexural failure of the hybrid (ST/CF) beam

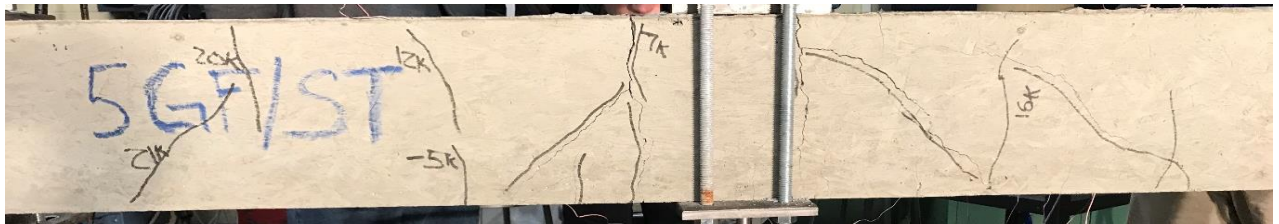


Fig. 22. Flexural failure of the hybrid (ST/GF) beam

3.3 Cracking behavior

Table 6 shows the crack details. The method described in [57] was used to find crack density as another ductility indication. The crack density was calculated using Eq. (1). Crack density results are shown in Fig. 23. The following paragraphs have a detailed description of the cracking observations during the experimental work.

$$\text{Crack Density} = \frac{\sum_{i=1}^n L_i \cdot W_i}{d} \tag{1}$$

Where, L_i is the length of the crack, W_i is the width of the crack, n is the number of cracks, and d is the beam depth.

The controlled beam (ST) showed its first crack at a load of 41 kN (9.2 kips) (around 38% of its peak load), and conforming to a displacement of 3.59 mm. (0.14 in.). While the test is proceeding, the flexural crack at the mid-span becomes wider until it fails at a deflection of 18.66 mm. (0.73 in.). This specimen had shown the highest ductility behavior, Fig. 18. On the other hand, CFRP and GFRP beams had evenly spread-out cracks suddenly before the failure when the FRP delaminated, Fig. 18 and Fig. 19. For the hybrid (ST/FRP) beams, the first crack was observed at around 40% of their failure load due to the existence of reinforcement, which gave them more ductility than FRP beams.

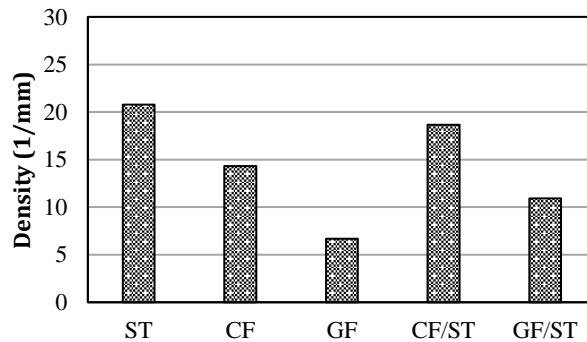


Fig. 23. Cracks density results

As can be seen from **Fig. 23**, the control beam has shown the highest ductility results compared to FRP specimens. The results obtained in this section, based on the approximate method, conforming to the results obtained using the ductility index.

Table 6. Cracks details

Beam ID	Average Crack Spacing mm. (in.)	Average Crack Width mm. (in.)	Number of Cracks	Cracks Density mm ⁻¹
PC	144.78 (5.7)	6.35 (0.250)	5	20.77
CF	157.48 (6.2)	2.56 (0.101)	8	14.30
GF	203.20 (8.0)	3.58 (0.141)	4	6.69
PC/CF	116.84 (4.6)	1.93 (0.076)	15	18.66
PC/GF	106.68 (4.2)	2.26 (0.089)	9	10.93

4. Mechanistic model for predicting flexural capacity of FRP grid reinforced beams

This section presents the analysis of the results based on the mechanistic models adopted from the ACI 318 [56]. The ACI 318 does not provide a prediction equation for high strength beams reinforced with FRP grid, therefore the authors used the available normal reinforced concrete beams’ ultimate flexural capacity equations to predict the nominal capacity of all beams presented in this study. However, the ACI 440R [58] presents the state of the art of FRP reinforcement, and it does not provide any mechanistic models to predict the behavior of high strength concrete beams reinforced with FRP grids. The authors used [58] as a guide to help in calculating the nominal capacity of the hybrid beams (4 and 5) presented in this study. The nominal capacity of beams 1, 2 and 3 have been calculated based on [56] as shown below:

In Eq. (2), M_{nfrp} is the nominal moment provided by the FRP only and M_{ns} is the nominal moment provided the steel. There moment capacities are calculated using the Eq. (3) to Eq. (5) below.

$$M_n = M_{ns} + M_{nfrp} \tag{2}$$

$$M_{nfrp} = T_{frp} * d_{frp} \tag{3}$$

$$T_{frp} = \epsilon_{frp} * A_{frp} * E_{frp} \tag{4}$$

$$A_{frp} = n_{frp} * t_{frp} * b_{frp} \tag{5}$$

The calculations of moment capacity was based on the allowable strain in the FRP grid, ϵ_{frp} , which depends on the mode of failure. The ACI 440 correlated the mode of the failure to the concrete crushing strength, steel yielding stress, and the rupture of FRP bars/grid. In addition, the ACI 440 differentiates between the delamination and the depending on FRP bars/grid from the surrounding concrete.

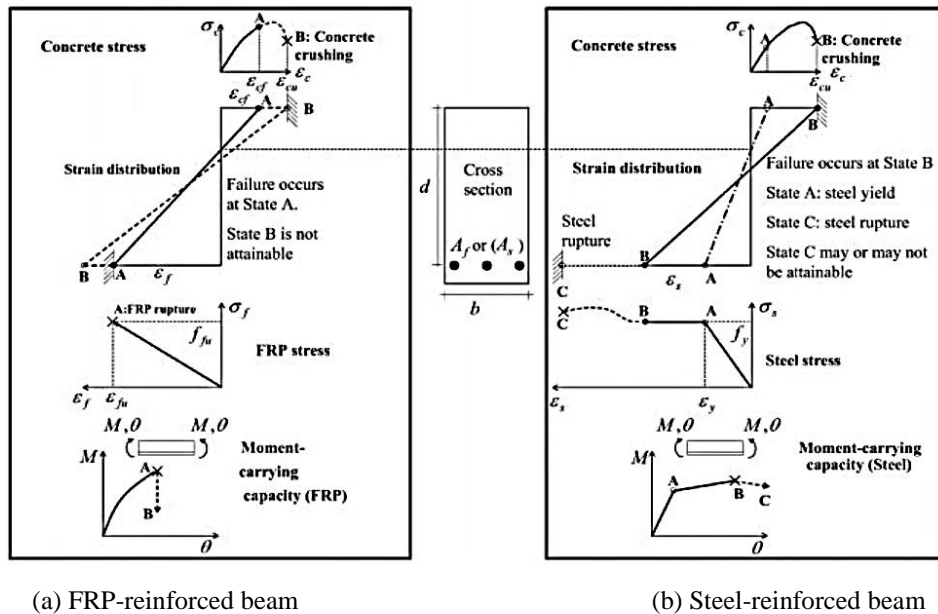


Fig. 24. Stress-Strain Relationship in FRP and Steel Reinforced Beams [56]

Fig. 24 shows the basics of the stress-strain relationship in FRP and steel beams. The main target of the design of such beams is to avoid sudden failure and provides enough ductility before failure.

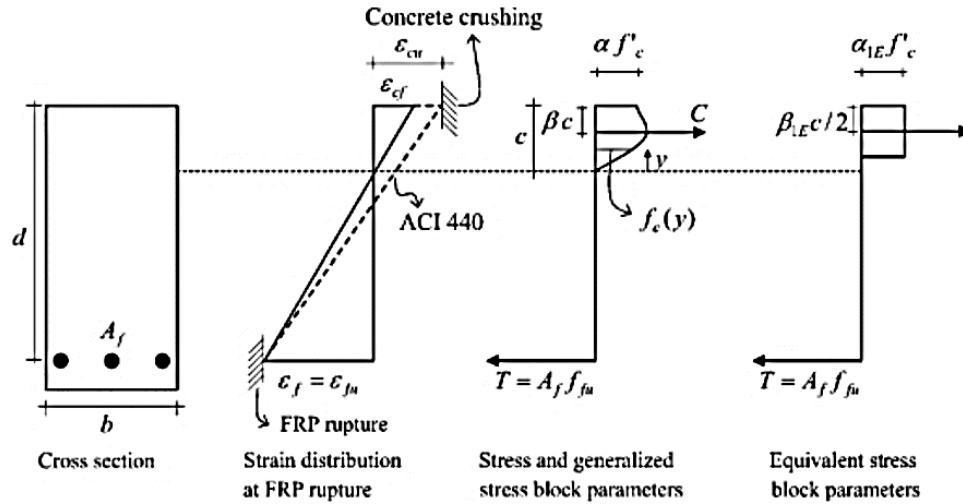


Fig. 25. Stress Block Diagram for Section Analysis [56]

In this study, the allowable tensile strain of FRP was taken equal to the debonding strain [58], where it was used to find the nominal strength of the FRP (equation 4). The equivalent stress block was used in the analysis and the compression reinforcement was neglected in the calculations as shown in Fig. 25. The area of reinforcement included both the steel and the FRP. Equations 6 to 8 presents the section equilibrium and the forces considered in the analysis. α was taken as 1.25 to account for strain hardening and α_1 as 0.65 based on the strength of the concrete.

$$C = T_s + T_{frp} \tag{6}$$

$$C = \alpha_1 * f'_c * A_c \tag{7}$$

$$T_s = \alpha * f_y * A_s \tag{8}$$

Table 7. Experimental and Mechanistic Models Moment Capacities

Code Used:	Experimental	ACI 318-14 (Material Properties)	ACI 318-14 (60% FRP strength)	ACI 440R
Specimen	ϕM_n [kip*ft]	ϕM_n [kip*ft]	ϕM_n [kip*ft]	ϕM_n [kip*ft]
1 Control	21.48	22.7	N/A	N/A
2 Carbon Fiber	18.03	30.5	18.7	N/A
3 Glass Fiber	8.84	12.4	7.5	N/A
4 CF + Steel	24.97	49.3	40.0	43.2
5 GF + Steel	21.05	32.8	28.6	33.2

Three models have been adopted from the ACI 318 and ACI 440R. One model used the whole FRP tensile strength and the second model assumed only 60% of the FRP tensile strength and the third model was based on [58]. It was shown that the second model showed results that were in good agreement with the experimental results. Equations 9 to 11 shows the steps to calculate the nominal moment strength. Table 7 shows the calculated moment capacities for all three models. For example, beam 4 (CF+steel) showed the moment capacity of 24.97 k.ft, 49.3 k.ft, 40 k.ft., and 43.2 k.ft for the experimental, ACI 318 and the 60% FRP strength and the ACI 440R, respectively.

$$\alpha = \frac{A_s \cdot f_y}{0.85 \cdot f'_c \cdot b} \tag{9}$$

$$f_{yfrp} = 0.6 f_{ufrp} \tag{10}$$

$$M_n = 0.85 f_{yfrp} \cdot A_{frp} \left(d - \frac{a}{2} \right) \quad (11)$$

5 Conclusions

The main goal of this study was to investigate the structural response of high strength concrete beams using fiber reinforced polymers under reversed cyclic loading. Five beams have been tested experimentally. The compressive strength of the used concrete was 8.5 ksi. The control beam was reinforced only by conventional steel bars, while other beams were reinforced with FRP and GFRP grids and with hybrid reinforcement. The results of the analysis were used to draw the following conclusions:

The CF and GF grids were practically used in high strength concrete beams as main reinforcement.

Beams included CF and GF showed more strength degradation (stiffness reduction) compared to the control beam.

The nominal moment capacity of hybrid reinforced beams were 138%-238% higher than the moment capacity of beams reinforced only by CF or GF grid.

The ductility index has been calculated for the control beam and the hybrid beams only, while other beams reinforced with CF and GF grids only had no ductility index due to the no yield point provided by the CF or the GF grid.

Hybrid beams still show good ductility indices (larger than 1.0) of 1.94 and 1.7 for the CF and GF, respectively.

Beams reinforce only with CF and GF showed moment capacity that 98% and 48% less than the capacity of the control beam.

Hybrid beams showed more number of cracks at failure, however the crack spacing was approximately less (75% and 88%) compared to the CF and GF only reinforced beams, respectively.

The mechanistic models of the ACI 318 (60% of FRP tensile strength) showed good agreement with the experimental results.

The mechanistic models of the ACI 440R, overestimated the nominal moment capacity of the hybrid beams.

The deflection of the ACI 318 and the 60% of FRP tensile strength methods, showed less values (25% - 88%) compared to the experimental results.

Finally, the ductility indices based on the ACI 318 were underestimated (58% - 67%) compared to the experimental results.

Acknowledgement

This work acknowledges the recourses offered by the Department of Civil and Environmental Engineering at the University of Idaho.

CRedit authorship contribution statement

Mohamed Elshazli: Investigation, Formal analysis, Writing – original draft. **Nick Saras:** Investigation, Formal analysis, Writing – original draft. **Ahmed Ibrahim:** Conceptualization, Funding acquisition, Supervision, Investigation, Formal analysis.

Conflicts of Interest

The authors declare that they have no conflicts of interest to report regarding the present study.

References

- [1] Carpenter, James E. Applications of high-strength concrete for highway bridges. *Public Roads* 1980; 44(2): 76-83.
- [2] Zia P, Schemmel JJ, Tallman TE. Structural applications of high-strength concrete. North Carolina Center for Transportation Engineering Studies 1989; FHWA-NC-89-006, Raleigh, North Carolina. <https://trid.trb.org/view/1181522>.
- [3] Kovacic D. Design of high strength concrete columns; Ed Mendis P. *Proceedings - high performance*

- concrete. University of Melbourne 1994; 86-116 Australia.
- [4] Xu P, Fu X, Wang C, Xiao C. Structural design of complex high rise building. Beijing: China Architecture & Building Press 2005; ISBN: 7112071240. (in Chinese).
 - [5] Xu P, Dai G. Performance-based seismic design of tall building structures beyond the code-specific ation. China Civil Engineering journal 2005; 38(1): 1-10. (in Chinese) <http://dx.doi.org/10.3321/j.issn:1000-131X.2005.01.001>.
 - [6] Bisby LA. Application and handling of frp reinforcements for concrete (Educational Module 6). ISIS Canada 2006. <https://www.mendeley.com/catalogue/48b52aeb-021f-3b82-a639-6e42bbf884ae/>.
 - [7] Idris Y, Ozbakkaloglu T. Flexural behavior of FRP-HSC-steel composite beams. Thin-Walled Structures 2014; 80: 207-216. <http://dx.doi.org/10.1016/j.tws.2014.03.011>.
 - [8] Lim JC, Ozbakkaloglu T. Influence of silica fume on stress-strain behavior of FRP-confined HSC. Construction and Building Materials 2014; 63(JUL.30):11-24. <http://dx.doi.org/10.1016/j.conbuildmat.2014.03.044>.
 - [9] Erfan AM, Elnaby R, Badr AA, El-Sayed TA. Flexural behavior of HSC one way slabs reinforced with basalt FRP bars. Case Studies in Construction Materials 2021; 14(5): 00513. <https://dx.doi.org/10.1016/j.cscm.2021.e00513>.
 - [10] Hadi MN. The behaviour of FRP wrapped HSC columns under different eccentric loads. Composite Structures, 2007; 78(4): 560-566. <http://dx.doi.org/10.1016/j.compstruct.2005.11.018>.
 - [11] Elshazli MT, Ramirez K, Ibrahim A, Badran M. Mechanical, durability and corrosion properties of basalt fiber concrete. Fibers, 2022; 10(2): 10. <https://dx.doi.org/10.3390/fib10020010>.
 - [12] Barbieri G, Biolzi L, Bocciarelli M, Cattaneo S. Size and shape effect in the pull-out of FRP reinforcement from concrete. Composite Structures 2016; 143: 395-417. <https://dx.doi.org/10.1016/j.compstruct.2016.01.097>.
 - [13] Berg AC, Bank LC, Oliva MG, Russell JS. Construction and cost analysis of an FRP reinforced concrete bridge deck. Construction and Building Materials 2006; 20(8): 515-526. <https://dx.doi.org/10.1016/j.conbuildmat.2005.02.007>.
 - [14] Kara IF, Ashour AF, K ro lu MA. Flexural behavior of hybrid FRP/steel reinforced concrete beams. Composite Structures 2015; 129: 111-121. <http://dx.doi.org/10.1016/j.compstruct.2015.03.073>.
 - [15] Rajkumar K, Vasumathi AM. Flexural behavior of fiber reinforced concrete beams confined with FRP. Applied Mechanics and Materials 2013; 256-259 (2013): 38-941. <http://dx.doi.org/10.4028/www.scientific.net/AMM.256-259.938>.
 - [16] Wang Y, Lee M, Chen B. Experimental study of FRP-strengthened RC bridge girders subjected to fatigue loading. Composite structures 2007; 81(4): 491-498. <https://dx.doi.org/10.1016/j.compstruct.2006.09.012>.
 - [17] Dong J, Wang Q, Guan Z. Structural behaviour of RC beams externally strengthened with FRP sheets under fatigue and monotonic loading. Engineering Structures 2012; 41: 24-33. <http://dx.doi.org/10.1016/j.engstruct.2012.03.024>.
 - [18] Qureshi M, Tandel Y, Patel B. An experimental study on high strength concrete using fly ash and alccofine. I-Manager's Journal on Structural Engineering 2013; 2(4): 1. <http://dx.doi.org/10.26634/jste.2.4.2752>.
 - [19] Salah-Eldin A, Mohamed HM, Benmokrane B. Axial-flexural performance of high-strength-concrete bridge compression members reinforced with basalt-FRP bars and ties: Experimental and theoretical investigation. Journal of Bridge Engineering 2019; 24(7): 04019069. [https://dx.doi.org/10.1061/\(ASCE\)BE.1943-5592.0001448](https://dx.doi.org/10.1061/(ASCE)BE.1943-5592.0001448).
 - [20] Aa A, Sga B, Zza B, Csa B, Dza B. A review on durability of fiber reinforced polymer (FRP) bars reinforced seawater sea sand concrete. Construction and Building Materials 2020; 256: 119484. <https://dx.doi.org/10.1016/j.conbuildmat.2020.119484>.
 - [21] Gudonis E, Timinskas E, Gribniak V, Kaklauskas G, Arnautov AK, et al. FRP reinforcement for concrete structures: state-of-the-art review of application and design. Engineering Structures and Technologies 2013; 5(4): 147-158. <https://dx.doi.org/10.3846/2029882X.2014.889274>.
 - [22] Chen Y, Davalos JF, Rey I, Kim HY. Accelerated aging tests for evaluations of durability performance of FRP reinforcing bars for concrete structures. Composite Structures 2007; 78(1): 101-111. <https://dx.doi.org/10.1016/j.compstruct.2005.08.015>.
 - [23] Altalmas A, Elrefai A, Abed F. Bond degradation of basalt fiber-reinforced polymer (BFRP) bars exposed to accelerated aging conditions. Construction and Building Materials 2015; 81: 162-171. <https://dx.doi.org/10.1016/j.conbuildmat.2015.02.036>.
 - [24] Wang Z, Zhao XL, Xian G, Wu G, Raman R, et al. Durability study on interlaminar shear behavior of basalt-, glass-and carbon-fiber reinforced polymer (B/G/CFRP) bars in seawater sea sand concrete environment. Construction and Building Materials 2017; 156: 985-1004. <https://dx.doi.org/10.1016/j.conbuildmat.2017.09.045>.
 - [25] Wang Z, Zhao XL, Xian G, Wu G, Raman R, et al. Effect of sustained load and seawater and sea sand concrete environment on durability of basalt-and glass-fiber reinforced polymer (B/GFRP) bars. Corrosion

- science 2018; 138: 200-218. <http://dx.doi.org/10.1016/j.corsci.2018.04.002>.
- [26] Guo F, Al-Saadi S, Raman R, Zhao XL. Durability of fiber reinforced polymer (FRP) in simulated seawater sea sand concrete (SWSSC) environment. *Corrosion Science* 2018; 141: 1-13. <https://dx.doi.org/10.1016/j.corsci.2018.06.022>.
- [27] Hassan M, Benmokrane B, Elsafty A, Fam A. Bond durability of basalt-fiber-reinforced-polymer (BFRP) bars embedded in concrete in aggressive environments. *Composites Part B: Engineering* 2016; 106: 262-272. <https://dx.doi.org/10.1016/j.compositesb.2016.09.039>.
- [28] Li Y, Zhao X, Raman R.S, Mechanical properties of seawater and sea sand concrete-filled FRP tubes in artificial seawater. *Construction and building materials* 2018; 191: 977-993. <https://dx.doi.org/10.1016/j.conbuildmat.2018.10.059>.
- [29] Sawpan MA. Shear properties and durability of GFRP reinforcement bar aged in seawater. *Polymer Testing* 2019; 75: 312-320. <https://dx.doi.org/10.1016/j.polymertesting.2019.02.033>.
- [30] Wang Z, Zhao XL, Xian G, Wu G, Raman R, et al. Long-term durability of basalt-and glass-fiber reinforced polymer (BFRP/GFRP) bars in seawater and sea sand concrete environment. *Construction and Building Materials* 2017; 139: 467-489. <https://dx.doi.org/10.1016/j.conbuildmat.2017.02.038>.
- [31] El-Hassan H, El-Maaddawy T, Abdelrahman, Al-Sallamin, Abdullah, et al. Performance evaluation and microstructural characterization of GFRP bars in seawater-contaminated concrete. *Construction and Building Materials* 2017; 147: 66-78. <https://dx.doi.org/10.1016/j.conbuildmat.2017.04.135>.
- [32] Cousin P, Hassan M, Vijay PV, Robert M, Benmokrane B. Chemical resistance of carbon, basalt, and glass fibers used in FRP reinforcing bars. *Journal of Composite materials* 2019; 53(26-27): 3651-3670. <https://dx.doi.org/10.1177/0021998319844306>.
- [33] Institute AC. Guide for the design and construction of structural concrete reinforced with fiber-reinforced polymer (FRP) bars. (ACI 440.1 R-15) 2015; American Concrete Institute Farmington Hills, Michigan.
- [34] Gravina RJ, Smith ST. Flexural behavior of indeterminate concrete beams reinforced with FRP bars. *Engineering Structures* 2008; 30(9): 2370-2380. <https://dx.doi.org/10.1016/j.engstruct.2007.12.019>.
- [35] Association CS. Design and construction of building structures with fiber-reinforced polymers. Canadian Standards Association 2012.
- [36] Reichenbach S, Preinstorfer P, Hammerl M, Kromoser B. A review on embedded fibre-reinforced polymer reinforcement in structural concrete in Europe. *Construction and Building Materials* 2021; 307: 124946. <https://dx.doi.org/10.1016/j.conbuildmat.2021.124946>.
- [37] El-Zeadani M, Saifulnaz M, Hejazi F, Amran Y, Jaafar MS, et al. Mechanics-based approach for predicting the short-term deflection of CFRP plated RC beams. *Composite Structures* 2019; 225: 111169. <https://dx.doi.org/10.1016/j.compstruct.2019.111169>.
- [38] Siddika A, Mamun M, Alyousef R, Amran M. Strengthening of reinforced concrete beams by using fiber-reinforced polymer composites: A review. *Journal of Building Engineering* 2019; 25: 100798. <https://dx.doi.org/10.1016/j.jobe.2019.100798>.
- [39] Amran Y, Alyousef R, Alabduljabbar H, Alaskar A, Alrshoudi, F. Properties and water penetration of structural concrete wrapped with CFRP. *Results in Engineering* 2020; 5: 100094. <https://dx.doi.org/10.1016/j.rineng.2019.100094>.
- [40] Ju M, Park K, Park C. Punching shear behavior of two-way concrete slabs reinforced with glass-fiber-reinforced polymer (GFRP) bars. *Polymers* 2018; 10(8): 893. <https://dx.doi.org/10.3390/polym10080893>.
- [41] Ascione L, Mancusi G, Spadea S. Flexural behavior of concrete beams reinforced with GFRP bars. *Strain* 2010; 46(5): 460-469. <https://dx.doi.org/10.1111/j.1475-1305.2009.00662.x>.
- [42] Bakar M, Rashid R, Amran M, Jaafar M, Vatin N, et al. Flexural strength of concrete beam reinforced with CFRP bars: A review. *Materials* 2022; 15(3): 1144. <https://dx.doi.org/10.3390/ma15031144>.
- [43] Rafi MM, Nadjai A, Ali F, Talamona D. Aspects of behavior of CFRP reinforced concrete beams in bending. *Construction and Building Materials* 2008; 22(3): 277-285. <https://dx.doi.org/10.1016/j.conbuildmat.2006.08.014>.
- [44] El-Zeadani M, Raizal MR, Amran YH, Hejazi F, Jaafar MS, et al. Analytical mechanics solution for measuring the deflection of strengthened RC beams using FRP plates. *Case Studies in Construction Materials* 2019; 11: e00272. <https://dx.doi.org/10.1016/j.cscm.2019.e00272>.
- [45] Shapira A, Bank LC. Constructability and economics of FRP reinforcement cages for concrete beams. *Journal of Composites for Construction* 1997; 1(3): 82-89. [https://dx.doi.org/10.1061/\(ASCE\)1090-0268\(1997\)1:3\(82\)](https://dx.doi.org/10.1061/(ASCE)1090-0268(1997)1:3(82)).
- [46] Cadenazzi T, Dotelli G, Rossini M, Nolan S, Nanni A. Cost and environmental analyses of reinforcement alternatives for a concrete bridge. *Structure and Infrastructure Engineering* 2020; 16(4): 787-802. <https://dx.doi.org/10.1080/15732479.2019.1662066>.
- [47] Li X, Hristov HA, Yee AF, Gidley DW. Influence of cyclic fatigue on the mechanical properties of amorphous polycarbonate. *Polymer* 1995; 36(4): 59-765. [https://dx.doi.org/10.1016/0032-3861\(95\)93105-U](https://dx.doi.org/10.1016/0032-3861(95)93105-U).
- [48] Brunner AJ, Stelzer S, Pinter G, Terrasi GP. Cyclic fatigue delamination of carbon fiber-reinforced polymer-

- matrix composites: Data analysis and design considerations. *International Journal of Fatigue* 2016; 83: 293-299. <https://dx.doi.org/10.1016/j.ijfatigue.2015.10.025>.
- [49] Vidjeapriya R, Jaya K. Experimental study on two simple mechanical precast beam-column connections under reverse cyclic loading. *Journal of Performance of Constructed Facilities* 2013; 27(4): 402-414. [https://dx.doi.org/10.1061/\(ASCE\)CF.1943-5509.0000324](https://dx.doi.org/10.1061/(ASCE)CF.1943-5509.0000324).
- [50] Fang I, Yen S, Wang C, Hong K. Cyclic behavior of moderately deep HSC beams. *Journal of Structural Engineering* 1993; 119(9): 2573-2592. [https://doi.org/10.1061/\(ASCE\)0733-9445\(1993\)119:9\(2573\)](https://doi.org/10.1061/(ASCE)0733-9445(1993)119:9(2573)).
- [51] Xiao Y, Ma R. Seismic behavior of high strength concrete beams. *The Structural Design of Tall Buildings* 1998; 7(1): 73-90. [https://dx.doi.org/10.1002/\(SICI\)1099-1794\(199803\)7:1<73::AID-TAL92>3.0.CO;2-A](https://dx.doi.org/10.1002/(SICI)1099-1794(199803)7:1<73::AID-TAL92>3.0.CO;2-A).
- [52] Xue W, Liang L, Cheng B, Jie L. The reversed cyclic load tests of normal and pre-stressed concrete beams. *Engineering structures* 2008; 30(4): 1014-1023. <https://dx.doi.org/10.1016/j.engstruct.2007.06.001>.
- [53] Sharbatdar MK. Monotonic and cyclic loading of new FRP reinforced concrete cantilever beams. 2008. <https://dx.doi.org/10.1109/TITS.2007.908721>.
- [54] Said AM, Nehdi ML. Performance of structural concrete frames reinforced with GFRP grid. Thirteenth world conference on earthquake engineering 2004. <http://ijce.iust.ac.ir/article-1-209-en.html>.
- [55] Yost JR, Goodspeed CH, Schmeckpeper ER. Flexural performance of concrete beams reinforced with FRP grids. *Journal of composites for construction* 2001; 5(1): 18-25. [https://dx.doi.org/10.1061/\(ASCE\)1090-0268\(2001\)5:1\(18\)](https://dx.doi.org/10.1061/(ASCE)1090-0268(2001)5:1(18)).
- [56] ACI Committee 318. Building code requirements for structural concrete (ACI 318-05) and commentary (ACI 318R-05). Farmington Hills, Mich. American Concrete Institute 2005. <https://www.doc88.com/p-990963918869.html>.
- [57] Eisa AS, Elshazli MT, Nawar MT, Experimental investigation on the effect of using crumb rubber and steel fibers on the structural behavior of reinforced concrete beams. *Construction and Building Materials* 2020; 252: 119078. <https://dx.doi.org/10.1016/j.conbuildmat.2020.119078>.
- [58] ACI 440R, 2007 Edition. Report on fiber-reinforced polymer (FRP) reinforcement for concrete structures 2007.

Publisher's Note: Sustainable Development Press Limited (SDPL) remains neutral with regard to jurisdictional claims in published maps and institutional affiliations.